Cell Membrane Alignment along Adhesive Surfaces: Contribution of Active and Passive Cell Processes

Anne Pierres, Philippe Eymeric, Emmanuelle Baloche, Dominique Touchard, Anne-Marie Benoliel, and Pierre Bongrand
INSERM U387, Laboratoire d'Immunologie, Hôpital de Ste-Marguerite, BP 29, 13274 Marseille Cedex 09, France

ABSTRACT Cell adhesion requires nanometer scale membrane alignment to allow contact between adhesion receptors. Little quantitative information is presently available on this important biological process. Here we present an interference reflection microscopic study of the initial interaction between monocytic THP-1 cells and adhesive surfaces, with concomitant determination of cell deformability, using micropipette aspiration, and adhesiveness, using a laminar flow assay. We report that 1), during the first few minutes after contact, cells form irregular-shaped interaction zones reaching ~100 μm^2 with a margin extension velocity of 0.01–0.02 μm/s. This happens before the overall cell deformations usually defined as spreading. 2), These interference reflection microscopic-detected zones represent bona fide adhesion inasmuch as cells are not released by hydrodynamic forces. 3), Alignment is markedly decreased but not abolished by microfilament blockade with cytochalasin or even cell fixation with paraformaldehyde. 4), In contrast, exposing cells to hypotonic medium increased the rate of contact extension. 5), Contacts formed in presence of cytochalasin, after paraformaldehyde fixation or in hypotonic medium, were much more regular-shaped than controls and their extension matched cell deformability. 6), None of the aforementioned treatments altered adhesiveness to the surface. It is concluded that adhesive forces and passive membrane deformations are sufficient to generate initial cell alignment to adhesive surfaces, and this process is accelerated by spontaneous cytoskeletally-driven membrane motion.

INTRODUCTION

Cell adhesion usually involves extensive reorganization of interacting surfaces. Indeed, whereas initial contact may involve an area of order of only 0.01 μm^2, corresponding to the tip of microvilli (Ben Shaul and Moscona, 1975; Grinnell et al., 1976; VonAndrian et al., 1995), a contact zone of several μm^2 containing thousands of adhesion receptors may appear within a few minutes (Foa et al., 1988; Dustin et al., 1996a,b; 1997). These deformations will result in membrane apposition, thus allowing contact between adhesion receptors whose length usually ranges between a few nanometers and a few tens of nanometers (Springer, 1990).

This process involves two complementary kinds of deformation. First, some reorganization of the cell surface must occur at the nanometer scale, as demonstrated and quantified in previous electron microscopical studies (Mège et al., 1987). Second, micrometer-scale deformations are required when a spherical cell flattens on a planar surface, resembling a liquid droplet. This flattening may precede more drastic deformations involving loss of radial symmetry and outgrowth of protrusions such as lamellipodia or filopodia, a phenomenon denominated as spreading that may be discriminated from adhesion on the basis of, for example, sensitivity to metabolic inhibitors or requirement for particular adhesive stimuli (Runyan et al., 1988; Lefkowitz et al., 1992; Watson et al., 2001).

Submitted May 29, 2002, and accepted for publication October 31, 2002.

Address reprint requests to Dr. Pierre Bongrand, INSERM U387, Laboratoire d'Immunologie, Hôpital Ste-Marguerite, BP29, 13274 Marseille Cedex 09 France. Tel.: +33-491-260-331; Fax: +33-491-757-328; E-mail: bongrand@marseille.inserm.fr.

0006-3495/03/03/2058/13 $2.00

Although many reports were devoted to the spreading process, quantitative information on the initial alignment of interacting surfaces at the nanometer level remains fairly scarce (Dustin et al., 1996a,b; Wülfing et al., 1998). Thus, it is not known whether this is a coordinated cellular process triggered by the very first intercellular bond or mechanical contact between membranes. Indeed, the possibility that a single molecular event might generate cell activation was reported in the somewhat extreme case of antigen recognition by T-lymphocytes (Sykulev et al., 1996). Alternatively, a study of the initial stage of integrin-mediated adhesion suggested the absence of cooperativity between binding events (Garcia and Boettiger, 1999). This result would be consistent with the hypothesis that alignment might first be driven by adhesive forces in absence of active cell participation (Bell et al., 1984). The potential of passive mechanisms to drive membrane alignment is well documented both experimentally and theoretically (Feder et al., 1995; Albersdörfer et al., 1997; Kloboucek et al., 1999; Boulbitch et al., 2001): soft vesicles bearing a combination of adhesion molecules and repulsive elements mimicking the cell glycocalyx were found to form an extended contact area with ligand-derivatized surfaces as monitored with quantitative interference reflection microscopy (IRM). However, it is not known whether reported patterns are quantitatively consistent with the behavior of actual cells, despite strong interest in applying wetting theory to bioadhesion (Bruinsma and Sackmann, 2001).

The aim of the present paper was to provide a quantitative description of the initial alignment of living cells to adhesive surfaces and assess the relative importance of active and passive phenomena during the initial step of adhesion. We studied the binding of human monocytic THP-1 cells to

polylysine-coated surfaces. These cells were chosen in view of information previously gathered on their mechanical properties (Richelme et al., 2000) as well as ideal adhesion kinetics inasmuch as alignment to the surface was completed within a few minutes. Polylysine was chosen as a nonspecific glue that was expected to bind to cell surfaces both uniformly and independently of their metabolic status. Also, previous reports were consistent with the hope that these nonspecific interactions might not generate specific biochemical signals (Haller et al., 1998; D'Souza-Schorey et al., 1998). Indeed, this surface treatment was found to induce adhesion without triggering extensive actin reorganization, even with highly excitable cells such as T-lymphocytes (Bunnell et al., 2001).

Fulfillment of our project required completion of the following steps: first, we derived a simple procedure for digital processing of IRM images to achieve objective determination of the boundaries of cell-surface contact areas. Indeed, although this microscopic technique was easily used to obtain qualitative information on cell-substrate interaction (Curtis, 1964; Bunnell et al., 2001), quantitative interpretation and thresholding is not straightforward (Gingell and Todd, 1979; Verschueren, 1985; Curtis, 1994) inasmuch as internal cell structures and surface membrane folds might significantly alter the expected relationship between local brightness and width of the cell-surface gap. Second, we studied the kinetics of contact extension during the first few minutes after contact between cell and adhesive surfaces. Third, active cell processes were altered by inhibiting active movements and decoupling the plasma membrane from underlying cytoskeletal elements with different treatments such as cytochalasin D, exposure to hypotonic medium or paraformaldehyde fixation, and the effect of these treatments on contact extension was quantified. Fourth, data interpretation was made possible by studying the effect of aforementioned treatments on membrane mechanical properties and adhesiveness: we performed micropipette aspiration and image analysis to measure the elastic component of membrane resistance to deformation. Also, a laminar flow chamber assay was used to discriminate between the effects of inhibitors on membrane adhesiveness and on cell capacity to fit to nearby surfaces.

It is concluded that adhesive forces and deformability-dependent membrane flattening are sufficient to initiate the formation of a significant contact area between a cell and an adhesive surface, and this process is strongly amplified by metabolism-dependent random cell surface movements.

MATERIALS AND METHODS

Cells and reagents

Human monocytic THP-1 cells (Tsuchiya et al., 1980) were propagated in RPMI 1640 medium supplemented with 20 mM HEPES, 10% FCS, 2 mM L-glutamine, 50 U/ml penicillin, and 50 U/ml streptomycin. Cells shared some typical properties of mononuclear phagocytes including active phagocytosis of opsonized erythrocytes, and surface expression of CD11b, CD18, CD29, CD32, CD35, CD43, CD45, CD64, and class I Major histocompatibility complex molecules, as assayed with flow cytometry.

In some cases, cells were treated with 1 or 10 μg/ml cytochalasin D (Sigma, St. Louis, MO).

Surfaces

Glass coverslips ($\sim 20 \times 6$ mm^2) were incubated for 4 h with concentrated sulphuric acid, then rinsed overnight with tap water, and washed with distilled water. They were then incubated with 0.1 mg/ml poly-L-lysine (ref. # P1524, mol wt 388,100) before a final wash in HEPES-buffered RPMI 1640 medium supplemented with 10% FCS.

In some cases, polylysine-coated coverslips were derivatized with fibronectin by 30-min incubation in a solution of 100 μM bis(sulfosuccinimidyl)suberate (BS^3, Pierce, ref. #21579, supplied by Interchim, Montluçon, France) and 100 nM fibronectin (human cellular fibronectin, Sigma, ref. #F 6277) in pH 7.2 phosphate buffer. Unreacted groups were then blocked with 0.2 M glycine for 15 min before extensive wash in PBS. A similar protocol was used to coat coverslips with anti-β1 monoclonal antibodies: fibronectin was replaced with 100 nM murine IgG1 monoclonal antibody (clone 3S3, Serotec France, Cergy-St. Christophe).

The surface density of fibronectin molecules was also studied on both types of coverslips following previously described methodology (Pierres et al., 2002). Briefly, mouse IgG1 antifibronectin antibodies were purified from culture supernatants of hybridoma HFN-7.1 (supplied by ATCC, ref. #CRL-1606) before labeling with fluorescein isothiocyanate. Coverslips were then incubated with 500 μg/ml fluorescent antibodies for 60 min at room temperature and washed in PBS supplemented with 0.2% bovine albumin. Surface fluorescence was measured with a Leica CLSM confocal microscope and calibrated with fluorescent antibody solutions of known concentration. The average surface density of fibronectin of coverslips treated with BS^3 technique was 12,500 molecules/μm^2. Interestingly, exposing polylysine-coated surfaces to fetal calf serum resulted in the appearance of a significant amount of 250 antifibronectin binding sites per μm^2.

Cytoskeletal labeling

Polymerized actin was labeled by incubating cells for 20 min at room temperature in presence of 3.7% paraformaldehyde, then for another 20-min period in phosphate buffer containing 10 U/ml bodipy phallacidin (Molecular Probes, Eugene, OR) and 0.1 mg/ml lysophosphatidylcholine (Sigma).

Static adhesion

Polylysine-coated coverslips were stuck with silicon glue to the bottom of a plexiglas block bearing a parallelepipedic cavity of $17 \times 6 \times 1$ mm^3 (Pierres et al., 1994; Sabri et al., 2000). THP-1 cells were then injected as 500,000 cells/ml suspensions in warm HEPES-buffered RPMI-1640 medium supplemented with 10% FBS. Chambers were deposited on an Axiovert 135 inverted microscope (Zeiss, Germany) equipped with an heating stage (TRZ 3700) set at 37°C. Interference reflection microscopy was performed with an antiflex objective (63× magnification, 1.25 NA). An H546 band-pass filter was inserted in the filter block in front of the beam splitter. Fluorescence observations were performed with standard fluorescein filters after microfilament labeling.

Images were obtained with an Hamamatsu C4742-95-10 CCD camera (10-bit accuracy) driven with HIPIC software. Under standard conditions, histogram expansion was performed to obtain high contrast images that were then stored as 1024×1024 pixel/8-bit depth TIF files. Further processing was performed with an image analysis software written in the laboratory

(André et al., 1990). More than 1000 files were stored to perform presented analyses.

In some experiments, the strength of cell-surface adhesion was assayed by driving culture medium into the chamber with a syringe, thus generating a wall shear stress of the order of 5–10 dyne/cm^2 during a few seconds. A cell of ~10 μm diameter would thus be subjected to a tangential force of the order of 100 piconewtons.

Determination of contact areas on microscopic images

Basic principles

The contrast of IRM images essentially results from the interference between rays I_1 and I_2 generated by reflection at the glass/medium and medium/cell interfaces respectively. Inasmuch as the index of refraction is lower in aqueous medium than in glass and cell bilayer, it results from Maxwell equations that there is a phase shift of $\pi(1 + 2d/\lambda)$ between I_1 and I_2, where d is the length of light path in medium and λ is the light wavelength in water. Assuming low incidence (i.e., d is about twice the distance δ between glass and the cell surface), the intensity I of the light ray generated by interferences between I_1 and I_2 is therefore given by the following relationship:

$$I = I_1 + I_2 - 2(I_1 I_2)^{1/2} \cos(4\pi\delta/\lambda). \quad (1)$$

After straightforward algebraic manipulation, Eq. 1 yields:

$$\delta = \lambda/4\pi \arccos[(2I - I_m - I_M)/(I_M - I_m)], \quad (2)$$

where I_m and I_M respectively stand for the minimal and maximal light intensities (corresponding to $\delta = 0$ and $\delta = \lambda/4$). The interest of Eq. 2 is that it remains valid if light intensities include an additive component due to spurious reflection. Also, it remains valid if contrast is enhanced by replacing the brightness I at any point by a linear combination ($aI + b$), where a and b are suitable constants used to combine background subtraction and contrast enhancement. However, it must be borne in mind that it is only an approximation, inasmuch as the low incidence assumption is not fully warranted (Gingell and Todd, 1979).

Contact determination

The major problem with IRM images obtained under standard conditions is a fairly low contrast. This is easily overcome by standard histogram expansion (an important point was to use a CCD camera yielding at least 1024 gray levels). Cell contacts thus appeared with sharp contrast. However, contrast enhancement also increased possible inhomogeneities of illumination intensity that might not be apparent on standard images. This was corrected by replacing the intensity I at any pixel of coordinates x,y with $I(1 + k_x x)(1 + k_y y)$, where constants k_x and k_y were chosen to minimize the brightness differences at the four corners of a 28 × 28 μm^2 area surrounding the cell.

The next step consisted of determining a threshold intensity to define contact areas. The threshold intensity I_t was derived from the maximum and minimum intensities I_M and I_m on each cell image according to the following formula:

$$I_t = 0.305\, I_M + 0.695\, I_m. \quad (3)$$

This equation was derived from Eq. 2 by taking 38.3 nm as threshold membrane-to-substrate separation (with a light wavelength of 410 nm in water, or 546 nm in vacuum). The derivation of this threshold value is described in the Results section (see Fig. 3).

A simple contour-follow algorithm (André et al., 1990) was then used to build contact areas. It was found useful to apply median filtering to contact images to get rid of artifactually dark isolated pixels.

Defining the complexity of contact areas

It was felt useful to build a quantitative parameter accounting for the ''complexity'' of contact areas. Indeed, in some cases, cell-to-substrate contact appeared as a single regular disc, whereas under other conditions contacts appeared as multiple irregular-shaped patches. We defined as a dimensionless complexity index C:

$$C = P^2/A, \quad (4)$$

where P is the number of pixels located at the boundary of contact zones (i.e., contact perimeter), and A is the total number of pixels in contact zone (thus representing contact area). C is usually less than 20 for a single regular patch, and it was higher than 200 in cells exhibiting very active contact formation.

Average velocity of contact extension

It appeared useful to determine the average velocity V of contact extension during a time interval Δt to allow quantitative test of models of membrane alignment. This was calculated with the formula:

$$V = \Delta A/(P\Delta t), \quad (5)$$

where ΔA is the variation of contact area during Δt and P is the perimeter of this area.

Dynamic adhesion

The laminar flow chamber provides a unique means of assessing intrinsic adhesiveness of the cell surface by excluding the possible influence of parameters such as deformability or lateral mobility of binding molecules. The principle consists in measuring the frequency of binding events between surfaces and cells driven by a hydrodynamic force of the order of a piconewton. Indeed, any significant adhesive interaction is expected to withstand a traction of a piconewton during at least several tenths of a second (Bongrand, 1999), thus resulting in a detectable arrest, independent of the cell capacity to strengthen adhesion through active processes such as membrane deformation, cytoskeletal reorganization, or receptor concentration in contact areas.

Measurements were conducted as previously described (Pierres et al., 1994; Sabri et al., 2000) by subjecting cell suspensions to a laminar shear flow generated by a syringe mounted on an electric syringe holder (the wall shear rate was calculated as $G = 6Q/h^2w$, where G is the flow rate, h the chamber height, and w the chamber width). Motion was recorded with a standard video camera (STM-M 108CE, Sony) mounted on an Olympus IX inverted microscope bearing a 40× long-distance objective. A wall shear rate of 2 s^{-1} was applied during a 10-min period and images were recorded for delayed analysis. Each experiment was replayed a sufficient number of times to observe the motion of at least 100 individual cells crossing a microscope field of 125 μm width. Arrest frequency was defined as the proportion of fully sedimented cells that exhibited at least one arrest during their passage across the microscope field.

Micromechanical studies

Cells were aspirated into micropipettes as previously described (Richelme et al., 2000). Briefly, micropipettes were prepared from borosilicate capillary tubes (0.8-mm internal diameter, Clark electromedical instruments, Phymep, Paris, France) with a programmable micropipette puller (model #773, Campden Instruments, Loughborough, UK) and enlarged to ~5-μm internal diameter with a deFonbrune microforge (Alcatel, Paris). Micropipettes were connected to a pressure generator made of a U-tube connected to a 2-ml syringe mounted on a micrometric holder. Pressure was continuously monitored with a sensor (Cole Parmer Instruments, Illinois, ref. #E 78300-04). Aspiration was performed on the stage of an Olympus IMT2 inverted

microscope, using a 40× dry objective (0.85 NA) and a 6.7× magnifying lens, together with a SIT video camera (model #4036, Lhesa, Cergy Pontoise, France). The output was connected to a PCVision+ digitizer (Imaging Technology, Bedford, MA) mounted on a desk computer. Digitized images were subjected to reverse digital-to-analog conversion, thus allowing real-time addition of time and pressure. A videotape recorder was used for continuous recording and delayed analysis.

In a typical experiment, cells were rapidly subjected to a pressure of 100 Pa in a standard medium made of 135 mM NaCl supplemented with 20 mM HEPES, 5 mM KCl, 1mM $MgCl_2$, 1mM $CaCl_2$, 10 mM glucose, and 0.1% bovine albumin.

Tapes were analyzed with standard image processing techniques (Richelme et al., 2000). Under standard conditions, 32 sequential images were stored with 5-Hz frequency for determination of the protrusion length with pixel accuracy (i.e., 0.27 μm).

RESULTS

Brightness variations on IRM images actually reflect cell-to-surface distance

A quantitative interpretation of IRM images may be impaired by 1), incomplete validity of the normal incidence approximation (Feder et al., 1995) and 2), possible influence of light reflection by intracellular organelles located close to the contact area. It was thus important to determine to what extent IRM gave reliable information on cell shape. This question was addressed by taking advantage of the property of THP-1 cells to remain fairly spherical when they are in suspension. Thus, a spherical cell that has just fallen in contact with the substratum was studied. Conventional and IRM images are shown in Fig. 1, *A* and *B*. The brightness variation along a line segment starting from the contact region is shown in Fig. 1 *C*. Equation 2 was used to calculate the cell-substratum distance δ when this was lower than $\lambda/4$ (λ is the light wavelength in water, i.e., 411 nm). Assuming that dark fringes represented circles where distance δ is a multiple of $\lambda/2$, other estimates of δ were obtained. Fig. 1 *D* shows that the calculated cell profile closely matched a circle, as expected.

Two conclusions may be drawn from this observation: first, IRM images clearly reflect the shape of cell boundary. Second, contrast is strongly decreased when cell-to-surface distance is higher than a quarter of a wavelength (Fig. 1 *C*). Therefore, in contrast with the predictions of Eq. 2, only contact areas can display a brightness close to the minimum. Thus, it should be in principle possible to define molecular contacts by simple thresholding of light intensities.

IRM images reveal actual adhesive contacts between cells and surfaces

Although it seems convincingly demonstrated that IRM images revealed areas of close apposition between cells and surfaces, a formal proof that these areas were indeed involved in adhesion was still lacking. To address this point, cells were first made to sediment on a surface and observed with conventional and interference reflection microscopy. They were then subjected to an hydrodynamic force of order of 100 pN. Finally, the same area was subjected again to microscopic examination. Typical images are shown on Fig. 2. Conclusions may be summarized as follows:

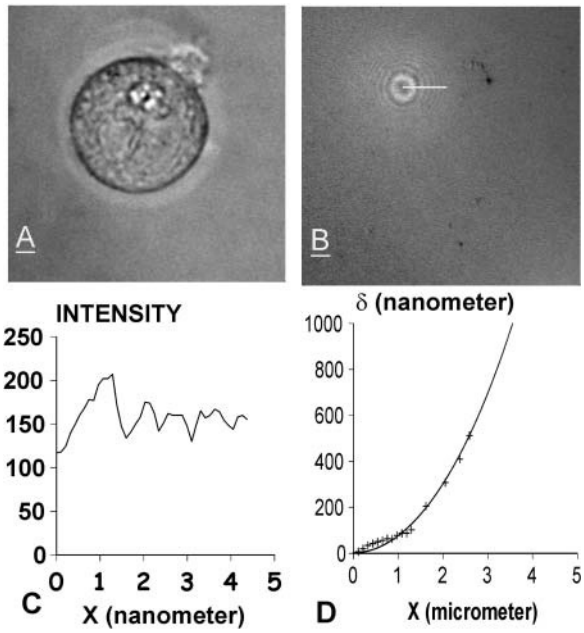

FIGURE 1 Derivation of cell membrane profile from IRM image. Monocytic THP-1 cells were made to sediment on polylysine-coated surfaces for ~2 min and subjected to microscopic examination. The conventional (*A*) and IRM (*B*) images of a representative cell are shown. The latter image displayed a set of concentric circles. The intensity profile along a radius (*white horizontal segment*) is shown in *C*. Equation 2 was used to derive the cell-surface separation distance δ (*inside the smallest dark circle*), and δ was taken as a multiple of $\lambda/4$ (where λ is the light wavelength) on dark circles. As shown in *D*, the calculated membrane profile (*crosses*) closely matched a circle (*continuous line*). Bar length is 2.5 μm in *A* and *B*.

- In some cases, the IRM image of cell/surface interaction area appeared as uniformly bright (Fig. 2 *B*, *white arrow*). This pattern suggested a lack of close cell-substrate apposition. As expected, these cells were always removed by hydrodynamic flow. Also, even in absence of flow, they sometimes displayed spontaneous Brownian-like motion, thus confirming the interpretation that they were not adherent
- In most cases, cells with dark IRM contacts resisted hydrodynamic forces and the IRM image remained essentially unaltered by this treatment. Fig. 2 represents a particularly informative example of a cell that displayed a moderate displacement in response to shear, with conservation of IRM contacts, suggesting that these contacts were actually adhesive and they were responsible for cell tethering to the initial binding zone (*black arrow*).
- Other images revealed dark IRM areas, but cells were removed by flow: in this case, some dark patches were still visible on IRM images after cell removal,

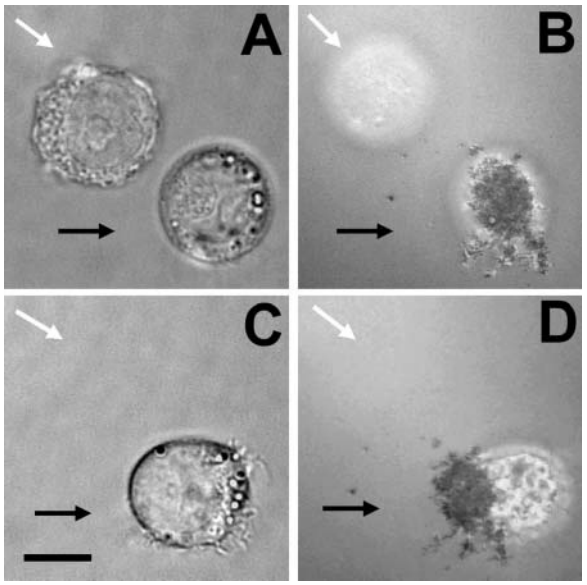

FIGURE 2 Dark zones on IRM images are indicative of cell-surface attachment. Monocytic THP-1 cells were deposited on polylysine-coated surfaces in a flow chamber and allowed to sediment for ten minutes. A representative field was chosen for recording conventional (*A*) and IRM (*B*) images. Cells were then subjected to a hydrodynamic flow generating a viscous drag of the order of 100 pN per cell. The conventional (*C*) and IRM (*D*) images of the same field were then recorded. As exemplified here, cells that yielded bright contact images under IRM conditions (*white arrow*) were always removed by the flow. On the contrary, most cells yielding dark contact (*black arrow*) resisted the flow. The cell shown here displayed limited displacement. Other cells were removed, leaving dark patches on the selected field (not shown). Bar length is 10 μm.

suggesting that these cells were adherent, but they were detached with membrane rupture when they were subjected to hydrodynamic forces (not shown).

It is thus concluded that contact areas revealed by IRM were actually involved in adhesion.

Contact areas may be derived from IRM images with simple thresholding algorithms

Inasmuch as our purpose was to perform a quantitative study of the time-evolution of cell/surface contacts, it was essential to build an algorithm allowing objective determination of these areas. Two procedures were compared and a typical example is shown in Fig. 3:

1. The histogram of intensity levels was built. As shown in Fig. 3 *C*, bimodal curves were obtained, suggesting that the intensity corresponding to the minimum between peaks might serve as a threshold between darker contact regions and brighter areas. This interpretation was supported by the finding that the histograms of images representing unbound cells (Fig. 2, *white arrows*) displayed a single peak (not shown).
2. The threshold was calculated following Eq. 3, using an empirical threshold distance to define contact.

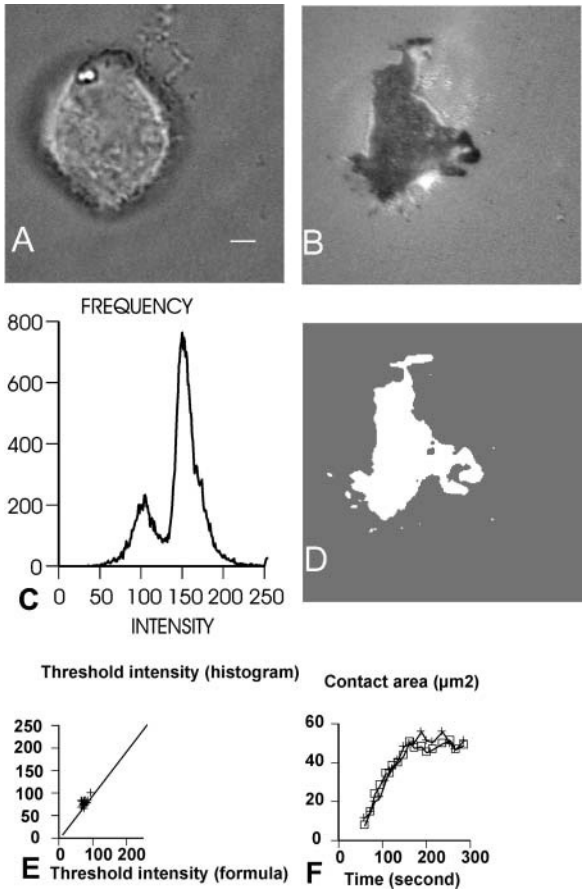

FIGURE 3 Determination of contact zones by processing IRM images. Conventional (*A*) and IRM (*B*) images of a representative THP-1 cell adhering to a polylysine-coated surface are shown. (*C*) The histogram of the IRM image is bimodal. (*D*) Darker pixels are located in a putative contact area appearing in white. In a series of 19 IRM images obtained on a typical cell at regular intervals of ~10 s, a threshold intensity between contact and noncontact pixels was obtained either by using the image histogram (as exemplified in *C*) or by using Eq. 2 with a threshold distance of 38 nm. Both procedures yielded highly correlated intensity thresholds (*E*), and contact areas obtained with histogram-based (*squares*) or formula-based (*crosses*) threshold yielded essentially identical estimates for the contact area (*F*).

As shown in Fig. 3 *E*, when procedures 1 and 2 were used to process a series of 19 images corresponding to the kinetics of contact formation between a single cell and the surface, they yielded closely related values when the theoretical threshold distance in Eq. 3 was set at 38.3 nm. Further, when both thresholding procedures were used to estimate the variations of the contact area, they yielded essentially similar curves (Fig. 3 *F*).

IRM reveals a rapid extension of cell-surface interaction during the first minutes after contact, in absence of typical spreading

In many separate experiments, THP-1 cells were deposited on adhesive surfaces and examined with standard and inter-

ference-reflection microscopy. A general conclusion was that during the first few minutes after contact, the IRM-defined interaction zone displayed marked extension whereas cells remained essentially rounded (Fig. 2, *A* and *B*, *black arrow*; Fig. 3, *A* and *B*). Only in a second phase initiated after ~10 min contact did typical spreading patterns appear such as filopodium or lamellipodium extension and loss of circular shape (Fig. 4). The purpose of the present work was to study the initial alignment of cell membranes to adhesive surfaces inasmuch as this appeared to play an essential role in initiating the adhesive process.

A first question was to know whether this alignment mainly involved the extension of an initial contact or formation of multiple cell-to-surface contacts with subsequent fusion. As exemplified in Fig. 5, both mechanisms seemed involved, with formation of new contacts in the vicinity of the main contact zone boundary and subsequent growth into irregular-shaped patches. The kinetics of contact increase as measured on a representative series of cells is displayed in Fig. 6.

Cell-surface contact maintenance does not require the presence of actin microfilaments

Inasmuch as previous IRM studies have revealed the frequent involvement of microfilaments in different contacts formed between spreading cells and surfaces, it was important to know whether polymerized actin was associated to initial contacts between THP-1 cells and surfaces. This question was addressed by studying microfilament organization during the first minutes after cell-surface contact. As exemplified in Fig. 7, a constant finding was that contact patches revealed by IRM contained no detectable fluorescence concentration; however, the contact boundary was surrounded by a region containing dense microfilament markers These observations suggested that the actin cytoskeleton might be involved in contact extension by pulling at the membrane, not in contact maintenance.

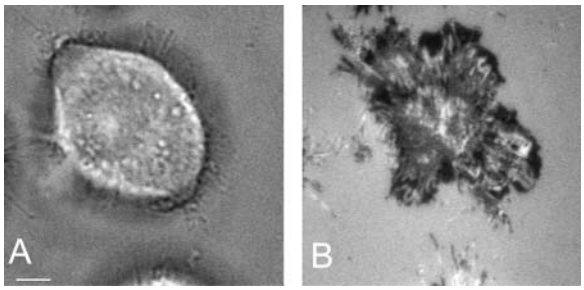

FIGURE 4 Cell spreading. When THP-1 cells were allowed to interact with polylysine-coated surfaces for more than 10–15 min, they began spreading with loss of rounded shape and emission of multiple lamellipodia or filopodia. Conventional (*A*) and IRM (*B*) images obtained on a typical cell are shown. Bar is 2.5 μm.

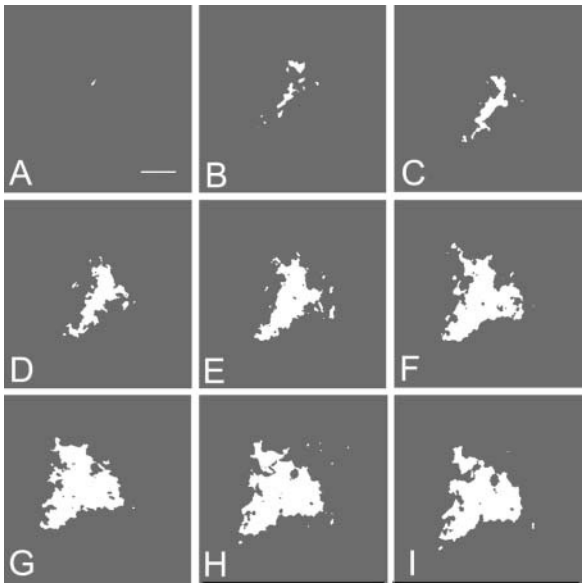

FIGURE 5 Morphological features of membrane alignment to an adhesive surface. A representative THP-1 cell was deposited on a polylysine-coated surface, and IRM images obtained at time 60 s (*A*), 83 s (*B*), 108 s (*C*), 123 s (*D*), 149 s (*E*), 173 s (*F*), 201 s (*G*), 237 s (*H*), and 267 s (*I*), were used to determine contact areas as explained. Bar length is 2.5 μm.

Cell-surface fitting may proceed in absence of active cell processes

Aforementioned results suggested studying the effect of different perturbations of cell metabolism on contact forma-

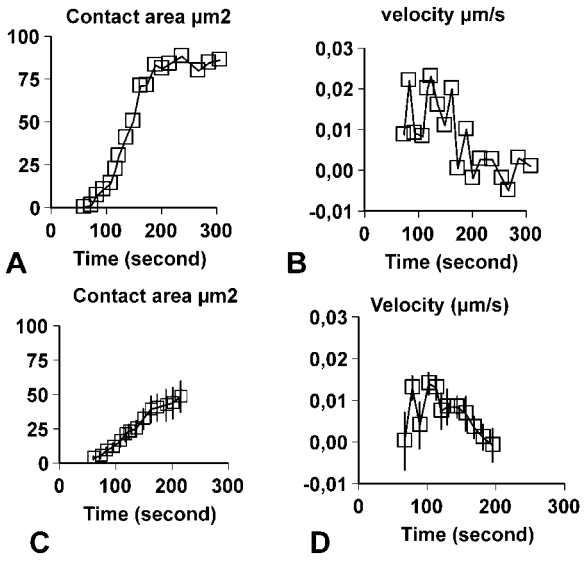

FIGURE 6 Kinetics of membrane alignment to adhesive surfaces. Monocytic THP-1 cells were deposited on polylysine-coated surfaces and IRM images were processed at regular intervals to determine the contact area (*A*, *C*) or linear velocity of the cell margin (*B*, *D*). Results obtained on a representative cell are shown (*A*, *B*) as well as mean values obtained on a series of five cells located on the same microscope field (*C*, *D*). Vertical bar length is twice the standard error.

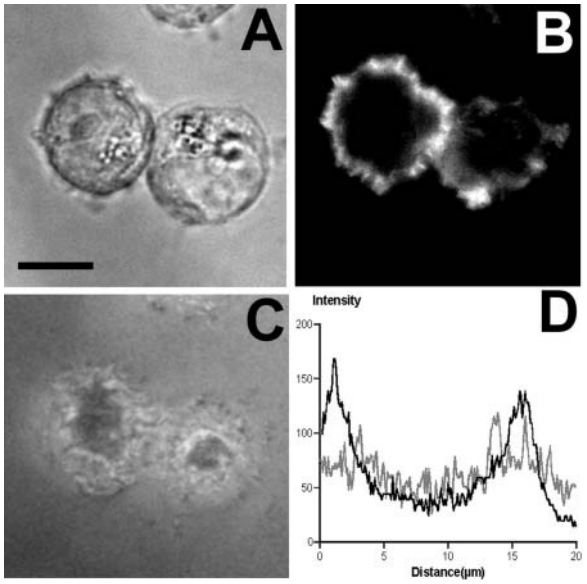

FIGURE 7 Microfilament distribution during contact formation. Monocytic THP-1 cells were deposited on polylysine-coated surfaces for adhesion and membrane alignment. Samples were fixed and labeled with fluorescent microfilament markers at regular intervals of 3–4 min. Images obtained by observing a typical field with conventional (*A*), fluorescence (*B*), or interference reflection (*C*) microscopy are shown. During the first minutes after contact, the IRM-defined contact did not contain any apparent fluorescent structure. The intensity profile along a vertical line of images (*B*) and (*C*) are shown on *D* as a thin and thick line, respectively: microfilaments are clearly located out of the contact zone. Bar length is 10 μm.

tion. The following three procedures were used: cells were treated with cytochalasin D to impair actin polymerization. They were fixed with paraformaldehyde to inhibit any active participation. Finally, they were exposed to hypotonic medium to change membrane mechanical properties.

A first requirement was to assess the effect of these treatments on cell adhesiveness to encountered surfaces, to be able to discriminate between this parameter and other factors likely to influence membrane alignment. This question was addressed by measuring the frequency of binding events between cells moving with very low velocity in a flow chamber and polylysine-coated surfaces, inasmuch as this binding was previously reported to be independent of active metabolic processes (Pierres et al., 1994). As shown in Table 1, cell adhesiveness was essentially unaffected by all performed treatments.

In contrast, as exemplified in Fig. 8, the three procedures we used dramatically altered the membrane alignment process: first, paraformaldehyde fixation essentially abolished cell-substrate apposition, inasmuch as only a few percent of cells displayed detectable contact areas after deposition on polylysine-coated surfaces, and these contacts remained limited (no more than a few μm^2 area) with a regular shape (Fig. 8 *B*). Second, cytochalasin treatment also decreased contact formation: inasmuch as most cells displayed significant alignment to surfaces, contact areas remained small and regular-shaped (Fig. 8 *D*). Third, exposure to hypotonic media resulted in dramatic increase of the rapidity and extent of contact formation (Fig. 8 *F*).

TABLE 1 Effect of different cell treatments on adhesiveness

Cell treatment	Number of counted cells	% Adhesion
Control	282	30.8 ± 2.8
Paraformaldehyde	73	38.3 ± 5.7
Cytochalasin D	157	35.7 ± 3.8
Hypotonic medium	77	35.1 ± 2.8

Monocytic THP-1 cells were driven along polylysine-coated surfaces in a laminar flow chamber in absence of treatment, or after treatment with 1% paraformaldehyde, or 10 μg/ml cytochalasin D, or in medium made hypotonic by adding 90% deionized water. The fraction of cells that were bound during their passage through a reference microscopic field was determined, and percentage of adhesion is shown together with calculated statistical error, as explained.

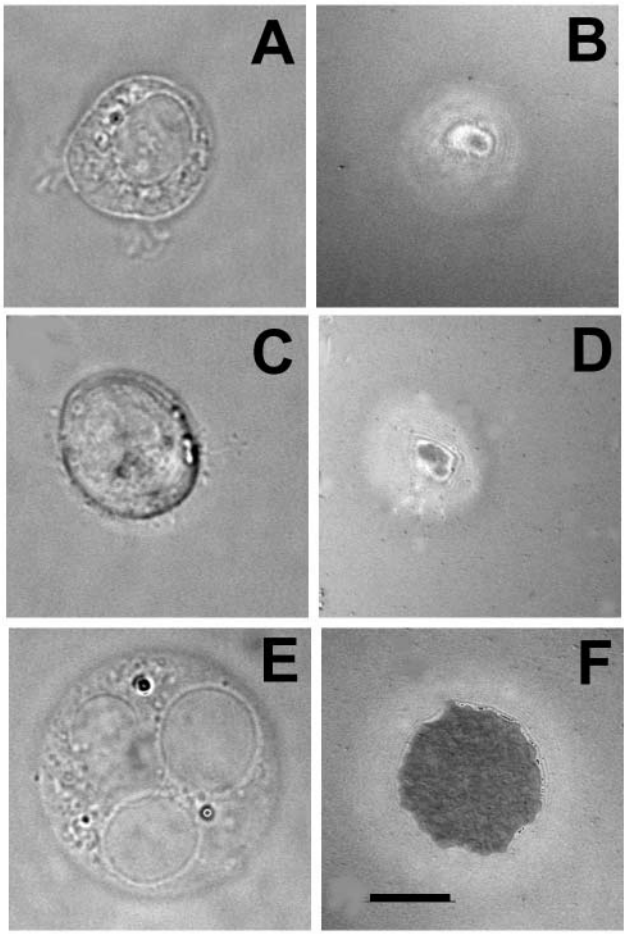

FIGURE 8 Pattern of contact formation between modified cells and adhesive surfaces. Cells were treated with 1% paraformaldehyde (*A*, *B*), 10 μM cytochalasin D (*C*, *D*), or hyposmotic medium (90% deionized water) before deposition of polylysine-coated surfaces and recording of conventional (*A*, *C*, *E*) or IRM (*B*, *D*, *F*) images. Bar length is 10 μm.

Similar cell behavior is found in absence of protein adsorption on adhesive surfaces

A potential problem in assessing the significance of our results was that serum adhesion proteins such as fibronectin were likely to be bound by polylysine-coated surfaces. Therefore, it was conceivable that adhesion and spreading be strongly dependent on the engagement of specific cell receptors, such as integrin fibronectin receptors. It was thus felt interesting to determine the influence of medium composition and surface preparation on contact formation.

First, cells were deposited on polylysine-coated surfaces in serum-free conditions. As shown in Fig. 9, contact formation was fairly similar to that observed in presence of serum. Contact extension was, however, slightly more rapid, with a maximum ~1 min after cell deposition, and cytochalasin D significantly decreasing the extent of spreading (Fig. 9, *B* and *D*).

Second, cells were deposited on surfaces pretreated with fibronectin, a ligand for THP-1 cell surface $\alpha_4\beta_1$ and $\alpha_5\beta_1$ integrins, in presence of serum: membrane alignment was markedly slower than found on polylysine-coated surfaces, inasmuch as maximal contact area was obtained only 45 min after cell deposition. Also, cell adhesion was strongly inhibited by cytochalasin D (not shown).

Third, when cells were deposited on surfaces that had been coated with anti-β_1 integrins, contact extension was completed within ~5 min. Further, cell-surface adhesion was not prevented by cytochalasin D (not shown).

Cytoskeletal impairment strongly decreases the extent and rapidity of cell spreading

The effect of metabolic alteration on the time course of contact extension was studied quantitatively.

As shown in Fig. 10 *A*, when cells were deposited on polylysine-coated surfaces in presence of serum, cytochalasin D treatment resulted in drastic decrease of contact extension. Thus, contact area was decreased eightfold as compared to controls after 5-min incubation. Conversely, contact extension was dramatically enhanced in hypotonic medium, with sevenfold increase after 5-min incubation. Finally, only a few percent of cells exhibited limited contact (as exemplified in Fig. 8, *A* and *B*) when they were treated with paraformaldehyde before contact initiation.

Results obtained in serum-free conditions are shown in Fig. 10 *B*: fitting was more rapid inasmuch as the contact time required to achieve 50% of plateau extension area was 95 s (Fig. 10 *B*) instead of 322 s (Fig. 10 *A*). Further, cytochalasin D also strongly decreased contact extension (eightfold decrease at 95 s and plateau), although a substantial contact area of 35 μm^2 could be obtained when microfilament function was impaired.

Contacts formed by cells subjected to metabolic alteration are much more regular-shaped than controls

Comparison of Figs. 5 and 8 suggests that contacts formed by unaltered cells were much more irregular than after metabolic alteration. This feeling was supported by a quantitative comparison of the dimensionless ratio between the squared perimeter and area of different cell populations. This parameter, that is, the one expected to account for the complexity of a surface, was 118 ± 32 SE ($n = 10$) on a series of control cells, and it was respectively 30.8 ± 3.9 SE ($n = 11$) and 41.5 ± 6.8 SE ($n = 7$) on cells exposed to cytochalasin D or hypotonic medium and made to spread in serum-containing medium. A similar trend was obtained under serum-free conditions inasmuch as the complexity parameter was respectively 205.2 ± 43 SE ($n = 5$) and 28.5 ± 4.0 SE ($n = 5$) in two representative sets of cells.

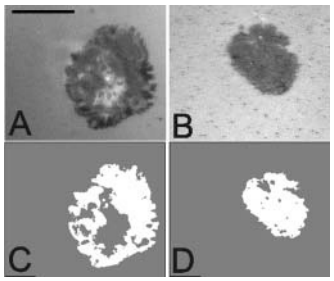

FIGURE 9 Contact formation in serum-free conditions. THP-1 cells were deposited on polylysine-coated surfaces in serum-free medium. A typical IRM image is shown on (*A*) together with contact (*C*). Experiments were repeated after treating cells with 10 μg/ml cytochalasin D, and a typical IRM image (*B*) and corresponding contact (*D*) are shown. Bar length is 2.5 μm.

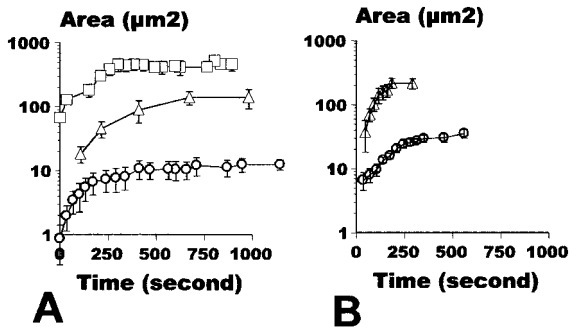

FIGURE 10 Kinetics of contact formation between cells and adhesive surfaces. Control THP-1 cells (*triangles*) or cells treated with 10 μm cytochalasin D (*circles*) or hypotonic medium (*squares*) were deposited on polylysine-coated surfaces and contact area was determined at regular intervals. Vertical bar length is twice the standard error (between 5 and 12 images). Experiments were performed in presence of (*A*) serum or (*B*) in serum-free conditions.

Cell capacity to align its membrane to an adhesive surface is partly correlated to passive deformability

Inasmuch as cell membrane alignment involves marked deformation of the cell surface, it was reasonable to look for a possible correlation between deformability and alignment capacity. Thus, control or metabolically altered cells were aspirated into micropipettes and deformation kinetics was monitored. Results are displayed in Fig. 11. Conclusions may be summarized as follows: first, in accordance with previous results (Richelme et al., 2000), cell aspiration resulted in rapid initial elastic deformation (within less than 200 ms) followed by a slower viscous-like elongation. Second, paraformaldehyde treatment rendered most cells undeformable, inasmuch as a few percent of assayed cells displayed initial elastic deformation, without further change during the following 150 s. Third, rather unexpectedly, cytochalasin treatment did not significantly affect cell mechanical properties as assayed during a 150-s period of time. Finally, exposure to hypotonic medium strongly increased cell deformability.

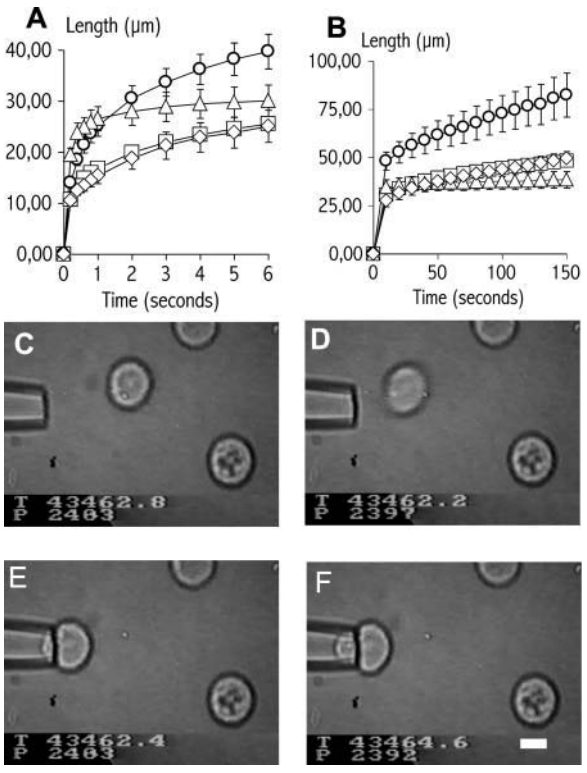

FIGURE 11 Deformability of THP-1 cells. Control (*squares*, 94 cells) THP-1 cells, or cells exposed to 10 μm cytochalasin D (*diamonds*, 23 cells), hypotonic medium (*circles*, 24 cells), or 1% paraformaldehyde (*triangles*, 10 cells) were aspirated into a glass micropipette with a pressure of 100 Pa and the length of evoked protrusion was repeatedly determined. The variations of protrusion length are shown during the first period of time (1–6 s, *A*) and up to 150 s after the onset of aspiration (*B*). Vertical bar length is twice the standard error. Representative images obtained during an experiment are shown (*C–F*). Bar length is 5 μm.

DISCUSSION

The main purpose of our work was to study the initial alignment of cell membranes to foreign surfaces as an early step of adhesion. Indeed, this fitting is a prerequisite to the formation of the minimal amount of bonds needed to ensure durable attachment, and we wished to know whether this process had to be triggered by some very early recognition event, or whether it might proceed as a consequence of active and/or passive uncoordinated membrane phenomena, thus resembling the adhesion of soft vesicles to adhesive surfaces.

A preliminary step was to validate an experimental procedure for accurate delineation of initial contacts between cells and surfaces. Inasmuch as IRM has long proved a valuable tool for qualitative observation of structures such as focal contacts and close contacts (Izzard and Lochner, 1976), and comparison with electron microscopy supported the view that IRM gave a satisfactory account of the distance between cell membranes and planar surfaces (Heath, 1982), it was not obvious that this technique might allow quantitative delineation of transient ''contact'' areas (Verschueren, 1985). Our results showed that this was indeed the case, inasmuch as 1), intensity/distance profiles obtained on cells of known structure (Fig. 1) suggested that contacts might be delineated with a simple thresholding procedure 2), an objective way of defining a correct threshold was provided (Fig. 3) and 3), combination of IRM and application of hydrodynamic forces unambiguously demonstrated a strong correlation between significant attachment and presence of IRM-defined contacts. The latter result is in line with a previous report from Dustin et al. (1996b) who used a parallel plate flow chamber to relate IRM to adhesion of T-lymphocyte hybridomas to surfaces coated with T-cell receptor ligand.

Extensive use of this analytical procedure yielded quantitative information on the first step of contact extension. During the first minutes after their encounter with an adhesive surface, cells displayed continuous growth of initial contacts with fairly irregular shapes and a margin velocity of the order of 0.01–0.02 μm/s. Interestingly, these features are not markedly different from the properties of contacts formed between artificial vesicles and moderately adhesive substrata (Feder et al., 1995), yielding very irregular interaction zones with a spreading velocity of the order of 0.1–0.2 μm/s. Also, when Albersdörfer et al. (1997) studied the interaction between biotinylated vesicles and surfaces in medium containing streptavidin (a multivalent biotin ligand), contact area increased for several hundreds of seconds with a typical margin velocity of the order of 0.01 μm/s (as obtained by quantitative analysis of Fig. 5 *a* of their paper). The shape of vesicle-surface contacts was also quite comparable to the images obtained in our model. Interesting data were also obtained by Kloboucek et al. (1999) in a later study of vesicle-surface adhesion mediated by CsA, an homophilic adhesion molecule incorporated in both interacting

surfaces. When the surface concentration of adhesive molecules was low, contacts remained patchy during hours, not unlike patterns displayed in our Figs. 3 and 5. In contrast, higher surface densities of adhesion receptors resulted in rapid merging of contacts resulting in a large rounded contact that indeed resembled that shown in Fig. 8 *F*. The patchy adhesion pattern was suggested to reflect a separation between receptor-rich areas, corresponding to contact, and regions enriched in antiadhesive polymers that had been incorporated in vesicles to mimic the cell glycocalyx (Bruinsma and Sackmann, 2001). Thus, marked similarities were found between our results and previous data obtained on artificial vesicles designed to mimic cell surfaces.

It was therefore warranted to investigate whether contact extension required active cell participation or if it was driven by passive thermally-driven surface deformations. A first way to address this problem consisted of studying the microfilament distribution during the first minutes after cell-surface contact. Interestingly, contact zones displayed uniformly low brightness but they were surrounded by a microfilament ring, in accordance with an earlier description of circumferential microfilaments appearing 3–5 min after plating polymorphonuclear neutrophils on surfaces (Boyles and Bainton, 1979). Although it is difficult to formally rule out the involvement of short-lived small microfilament bundles in contact extension, this possibility is not supported by our findings. Thus, three conclusions may be suggested: first, this pattern is at variance with the presence of an actin network in active lamellipodia (Rinnerthaler et al., 1991), suggesting that contact extension may not be driven by the same processes as lamellipodial extension; this is consistent with the finding that there existed several dynamical populations of actin polymers in spreading postmitotic PtK2 cells (Cramer and Mitchison, 1993). Second, the absence of microfilaments underlying cell membrane in contact areas is consistent with the possibility that this membrane might be free enough to display random fluctuations. Third, the presence of cytoskeletal elements in the periphery of contact areas made conceivable an extension mechanism based on peripheral traction.

Another way of elucidating the mechanisms of contact extension consisted of selectively altering cell active motility or passive membrane mechanical properties without modifying adhesiveness, and monitoring the effects of performed treatments on the fitting process. First, cytochalasin D dramatically decreased the rate of contact extension (Fig. 10). This could not be ascribed to a decrease of membrane adhesiveness inasmuch as the efficiency of cell attachment to polylysine-coated surfaces under flow was unaltered by this treatment. This result is significant inasmuch as the binding parameter obtained with this technique yields an accurate account of membrane adhesiveness rather than other cell functions possibly related to cell adhesion (such as, for example, spreading ability or mobility of membrane molecules). Indeed, the duration of contact formation under flow was of the order of 1 ms, which is too short to allow active cell participation (Pierres et al., 1994). Interestingly, cytochalasin treatment did not alter cell capacity to undergo passive deformation, as assayed with micropipette aspiration (Fig. 11). The simplest interpretation of these results is that the high rate of contact extension observed in control cells was due to active microfilament-dependent deformations of the cell membrane.

The lack of measurable effect of cytochalasin D treatment on cell mechanical properties deserves some comments: indeed, treating other leukocytic cells with cytochalasin B, a microfilament inhibitor, was previously found to increase cell deformation into micropipettes in our (Mège et al., 1985) or other (Tsai et al., 1994) laboratories. Also, cytochalasin treatment increased cell indentation obtained by exerting a controlled pressure with a glass tip (Petersen et al., 1982). Conversely, cytochalasin inhibited the formation of protrusion by micropipette-aspirated *Fundulus heteroclitus* egg cells (Tickle and Trinkaus, 1977). We suggest that the apparent discrepancy between these results might be due to a dual effect of microfilament inhibition on cell mechanical properties: this treatment might loosen the connection between the plasma membrane and underlying cytoskeleton, thus resulting in spontaneous blebbing (Juliano and Gagalang, 1977) and easier separation of the plasma membrane and cell cortical region by low mechanical forces (Raucher and Sheetz, 1999), thus increasing surface deformability. However, cytochalasin might also reduce the cytoskeleton capacity to reorganize itself and deform in response to external forces. This hypothesis is supported by a previous observation made in our laboratory (Richelme et al., 1997) that cytochalasin D decreased the long-term deformation of micropipette-aspirated THP-1 cells, as measured 150 s after the onset of aspiration, but not the initial rate of protrusion elongation, a result consistent with the nonsignificant trend suggested by Fig. 11 *B*.

However, experiments done with cytochalasin did not allow us to determine whether the slow and limited contact extension observed on treated cells deposited on polylysine-coated surfaces was driven by residual cell motility or whether it could be generated by an altogether passive mechanism. This problem was addressed by treating cells with 1% paraformaldehyde to abolish any active cell function. Results allowed unambiguous conclusions inasmuch as paraformaldehyde did not alter cell surface adhesiveness (Table 1). When cell-surface interaction was studied with IRM, only a minor fraction of cells displayed detectable contacts, and these contacts were comparable to those formed by cytochalasin-treated cells (Fig. 8). In agreement with these results, when cell mechanical properties were studied, only a minor fraction of cells formed protrusions when they were aspirated into micropipettes, and elongation kinetics displayed remarkable behavior, with rapid initial extension that stopped after 1–2 s (Fig. 11). Further, microscopic observation (not shown) suggested that a protrusion appeared only when the plasma membrane became separated from rigid inner structures

as previously observed on a proportion of control cells (Richelme et al., 2000). These observations demonstrate that limited contact extension may occur without any active cell participation, provided surface deformability is sufficient, thus allowing a behavior close to that of artificial vesicles (Feder et al., 1995; Boulbitch et al., 2001). It is tempting to speculate that this deformability might be enhanced by spontaneous separation between the plasma membrane and underlying cytoplasmic cortex. It must be emphasized that the possibility of plasma membrane separation from underlying structures was unambiguously demonstrated by several authors who reported on the formation of small membrane tethers when a local traction was applied to the cell surface (Shao and Hochmuth, 1996; Raucher and Sheetz, 1999; Sheetz, 2001).

To subject the above concept to further analysis, cells were tentatively exposed to hypotonic medium to modify surface tension without provoking drastic alteration of the cell metabolism. Indeed, although this treatment might induce some activation, as reported in other systems (Feranchak et al., 2001), it is not known to trigger marked increase of cell motility. First, hypotonic treatment did not change surface adhesiveness (Table 1). Second, it resulted in about sevenfold increase of the contact area obtained during the first minutes after surface encounter (Fig. 9). Interestingly, contacts were fairly circular (Fig. 8) with a far more regular shape than displayed with controls (Fig. 5). Third, hypotonic medium substantially increased cell deformability. This finding is in line with a recent report of the effect of osmotic stress on the mechanical properties of chondrocytes (Guilak et al., 2002), and it is consistent with the concept that hypotonic shock will release reserve membrane (Raucher and Sheetz, 1999), although a transient increase of membrane tension is also expected (Raucher and Sheetz, 2000). This interpretation is supported by our finding (not shown) that cell deformability increase was more clearcut after several-minute exposure to hypotonic medium. The simplest interpretation of these experiments would be that free membrane rapidly became aligned to the surface, yielding a fairly regular contact area. Increased contact might thus be due to increased frequency and amplitude of active cell deformation. It must be emphasized that it would not be a straightforward task to discriminate between increased passive deformability and increased random cell deformations, inasmuch as both processes may be linked to common cell structural properties.

Preliminary observations made on the interaction between cells and surfaces coated with fibronectin or anti-β_1 integrin antibodies are consistent with our conclusion that the fitting process may occur in absence of active cell movement, although with a somewhat decreased efficiency. The low rate of contact formation on fibronectin, a well-known ligand for CD29dCD49 and CD29eCD49 integrins, suggests that these receptors are not fully activated on THP-1 cells, although they are well expressed as checked with flow cytometry (not shown). Due to the low fitting efficiency in this system, it is not surprising that it was no longer detectable in presence of cytochalasin D. In contrast with these findings, the observation that contact extension was very rapid on surfaces coated with anti-β_1 integrin antibodies, and that it resisted cytochalasin D treatment, emphasizes the importance of binding kinetics and molecular accessibility on contact extension: indeed, antibodies act as a flexible spacer of $\sim$20 nm which may allow adhesion to occur at higher surface separation than with fibronectin. In this case, passive surface motion may be sufficient to drive rapid contact extension. It is certainly warranted to plan additional experiments to elucidate the relationship between receptor structure and contact extension.

In conclusion, the initial contacts formed between an adhesive surface and cells exposed to cytochalasin D, paraformaldehyde, or hypotonic medium were fairly circular, and their extension was positively correlated to cell deformability as assayed with micropipette aspiration. Untreated cells displayed more rapidly growing contacts, with irregular shape and qualitatively different growth pattern, inasmuch as new contacts continuously appeared at some distance from the main growing patch (Fig. 5). These results are consistent with the concept that the initial alignment of cells to adhesive surfaces, a key step toward the formation of strong attachment, may be initiated by the mere interplay of passive physical forces. However, this process would be concomitantly amplified by random deformation of the cell membrane, resulting in a qualitatively different contact pattern. This scheme does not require any coordinated cellular process, which might be related to the subsequent spreading stage of cell-substrate interaction. Further comparison of the behavior of cells and artificial vesicles should help unravel the intricacy of passive and actively coordinated phenomena that is often found in the analysis of cell behavior.

It must be emphasized that the results we obtained in this model do not disprove the possibility that specific molecular interactions in particular cell-cell interfaces might rapidly trigger contact development far more efficiently than might be accounted for by passive mechanisms alone. This is well illustrated by the formation of a so-called immunological synapse in the region of contact between T-lymphocytes and antigen-presenting cells (Grakoui et al., 1999; Bromley et al., 2001). Indeed, previous work done in our laboratory (André et al., 1990) convinced us that lymphocytes might be far more efficient than mononuclear phagocytes in achieving rapid and extensive redistribution of membrane receptors in contact areas.

REFERENCES

Albersdörfer, A., T. Feder, and E. Sackmann. 1997. Adhesion-induced domain formation by interplay of long-range repulsion and short-range attraction force: a model membrane study. *Biophys. J.* 73:245–257.

André, P., A. M. Benoliel, C. Capo, C. Foa, M. Buferne, C. Boyer, A. M. Schmitt-Verhulst, and P. Bongrand. 1990. Use of conjugates made between a cytolytic T cell clone and target cells to study the re-

distribution of membrane molecules in contact areas. *J. Cell Sci.* 97: 335–347.

Ben Shaul, Y., and A. A. Moscona. 1975. Scanning electron microscopy of aggregating embryonic neural retina cells. *Exp. Cell Res.* 95:191–204.

Bell, G. I., M. Dembo, and P. Bongrand. 1984. Cell adhesion: competition between nonspecific repulsion and specific bonding. *Biophys. J.* 45: 1051–1064.

Bongrand, P. 1999. Ligand-receptor Interactions. *Rep. Prog. Phys.* 62: 921–968.

Boulbitch, A., Z. Guttenberg, and E. Sackmann. 2001. Kinetics of membrane adhesion mediated by ligand-receptor interaction studied with a biomimetic system. *Biophys. J.* 81:2743–2751.

Boyles, J., and D. F. Bainton. 1979. Changing patterns of plasma-membrane associated filaments during the initial phases of polymorphonuclear leukocyte adherence. *J. Cell Biol.* 82:347–368.

Bromley, S. K., A. Iaboni, S. J. Davis, A. Whitty, J. M. Green, A. S. Shaw, A. Weiss, and M. L. Dustin. 2001. The immunological synapse and CD28–CD80 interactions. *Nat. Immunol.* 2:1159–1166.

Bruinsma, R., and E. Sackmann. 2001. Bioadhesion and the dewetting transition. *C. R. Acad. Sci. Paris Sér IV* 803–815.

Bunnell, S. C., V. Kapoor, R. P. Trible, W. Zhang, and E. Samelson. 2001. Dynamic actin polymerization drives T cell-receptor-induced spreading: a role for the signal transduction adaptor LAT. *Immunity*. 14:315–329.

Cramer, L., and T. J. Mitchison. 1993. Moving and stationary actin filaments are involved in spreading of postmitotic PtK2 cells. *J. Cell Biol.* 122:833–843.

Curtis, A. S. G. 1964. The mechanism of adhesion of cells to glass. *J. Cell Biol.* 20:199–215.

Curtis, A. S. G. 1994. Interference reflection microscopy and related microscopy and cell adhesion. *In* Studying Cell Adhesion. P. Bongrand, P. Claesson, and A. Curtis, editors. Springer, Heidelberg, 185–193.

D'Souza-Schorey, C., B. Boettner, and L. Van Aebst. 1998. Rac regulates integrin-mediated spreading and increased adhesion of T-lymphocytes. *Mol. Biol. Cell.* 18:3936–3946.

Dustin, M. L., L. M. Ferguson, P.-Y. Chan, T. A. Springer, and D. E. Golan. 1996a. Visualization of CD2 interaction with LFA-3 and determination of the two dimensional dissociation constant for adhesion receptors in a contact area. *J. Cell Biol.* 132:465–474.

Dustin, M. L., D. E. Golan, D. M. Zhu, J. M. Miller, W. Meier, E. A. Davies, and P. A. van der Merwe. 1997. Low affinity interaction of human or rat T cell adhesion molecule CD2 with its ligand aligns adhering membranes to achieve high physiological affinity. *J. Biol. Chem.* 272:30889–30898.

Dustin, M. L., J. M. Miller, S. Ranganath, D. A. A. Vignali, N. J. Viner, C. A. Nelson, and E. R. Unanue. 1996b. T cell receptor mediated adhesion of T cell hybrydomas to planar bilayers containing purified MHC class II/peptide complexes and receptor shedding during detachment. *J. Immunol.* 157:2014–2021.

Feder, T. J., G. Weissmüller, B. Zeks, and E. Sackmann. 1995. Spreading of giant vesicles on moderately adhesive substrates by fingering: a reflection interference contrast microscopy study. *Phys. Rev. E.* 51: 3427–3433.

Feranchak, A. P., T. Berl, J. Capasso, P. A. Wojtciszek, J. Han, and J. G. Fitz. 2001. p38 MAP-kinase modulates liver cell volume through inhibition of membrane Na^+ permeability. *J. Clin. Invest.* 108:1495–1504.

Foa, C., J. L. Mège, C. Capo, A. M. Benoliel, J. R. Galindo, and P. Bongrand. 1988. T-cell-mediated cytolysis: analysis of killer and target cell deformability and deformation during conjugate formation. *J. Cell Sci.* 89:561–573.

Garcia, A. J., and D. Boettiger. 1999. Integrin-fibronectin interactions at the cell-material interface: initial integrin binding and signaling. *Biomaterials.* 20:2427–2433.

Gingell, D., and I. Todd. 1979. Interference reflection microscopy: a quantitative theory for image interpretation and its application to cell-substratum separation measurement. *Biophys. J.* 26:507–526.

Grakoui, A., S. K. Bromley, C. Sumen, M. M. Davis, A. S. Shaw, P. M. Allen, and M. L. Dustin. 1999. The immunological synapse: a molecular machine controlling T cell activation. *Science*. 285:221–227.

Grinnell, F., M. Q. Tobleman, and C. R. Hackenbrock. 1976. Initial attachment of baby hamster kidney cells to an epoxy substratum. *J. Cell Biol.* 70:707–713.

Guilak, F., G. R. Erickson, and H. P. Ting-Beall. 2002. The effects of osmotic stress on the viscoelastic and physical properties of articular chondrocytes. *Biophys. J.* 82:720–727.

Haller, H., C. Lindschau, C. Maasch, H. Olthoff, D. Kurscheid, and F. C. Luft. 1998. Integrin-induced protein kinase alpha and C epsilon translocation to focal adhesions mediates vascular smooth muscle cell spreading. *Circ. Res.* 82:157–165.

Heath, J. P. 1982. Adhesions to substratum and locomotory behaviour of fibroblastic and epithelial cells in culture. *In* Cell Behaviour. R. Bellairs, A. Curtis, and G. Dunn, editors. Cambridge University Press, Cambridge. 77–108

Izzard, C. S., and L. R. Lochner. 1976. Cell-to-substrate contacts in living fibroblasts: an interference reflexion study with an evaluation of the technique. *J. Cell Sci.* 21:129–159.

Juliano, R. L., and E. Gagalang. 1977. The adhesion of Chinese hamster cells. I - Effects of temperature, metabolic inhibitors, and proteolytic dissection of cell surface macromolecules. *J. Cell. Physiol.* 92:209–220.

Kloboucek, A., A. Behrisch, J. Faix, and E. Sackmann. 1999. Adhesion-induced receptor segregation and adhesion plaque formation: a model membrane study. *Biophys. J.* 77:2311–2328.

Lefkowitz, J. B., M. R. Lennartz, M. Rogers, A. R. Morrison, and E. J. Brown. 1992. Phospholipase activation during monocyte adherence and spreading. *J. Immunol.* 149:1729–1735.

Mège, J. L., C. Capo, A. M. Benoliel, and P. Bongrand. 1987. Use of cell contour analysis to evaluate the affinity between macrophages and glutaraldehyde-treated erythrocytes. *Biophys. J.* 52:177–186.

Mège, J. L., C. Capo, A. M. Benoliel, C. Foa, and P. Bongrand. 1985. Study of cell deformability by a simple method. *J. Immunol. Methods.* 82:3–15.

Petersen, N. O., W. B. McConnaughey, and E. L. Elson. 1982. Dependence of locally measured cellular deformability on position of the cell, temperature, and cytochalasin B. *Proc. Natl. Acad. Sci. USA*. 79: 5327–5331.

Pierres, A., O. Tissot, B. Malissen, and P. Bongrand. 1994. Dynamic adhesion of CD8-positive cells to antibody-coated surfaces the initial step is independent of microfilaments and intracellular domains of cell-binding molecules. *J. Cell Biol.* 125:945–953.

Pierres, A., D. Touchard, A. M. Benoliel, and P. Bongrand. 2002. Dissecting streptavidin-biotin interaction with a laminar flow chamber. *Biophys. J.* 82:3214–3223.

Raucher, D., and M. P. Sheetz. 1999. Characteristics of a membrane reservoir buffering membrane tension. *Biophys. J.* 77:1992–2002.

Raucher, D., and M. P. Sheetz. 2000. Cell spreading and lamellipodial extension rate is regulated by membrane tension. *J. Cell Biol.* 148:127–136.

Richelme, F., A. M. Benoliel, and P. Bongrand. 1997. Mechanical deformation of monocytic THP-1 cells: occurrence of two sequential phases with differential sensitivity to metabolic inhibitors. *Exp. Biol. Online* 2:5. *First published on February. 20, 1997.*

Richelme, F., A. M. Benoliel, and P. Bongrand. 2000. Dynamic study of cell mechanical and structural responses to rapid changes of calcium level. *Cell Motil. Cytoskeleton.* 45:93–105.

Rinnerthaler, G., M. Herzog, M. Klappacher, H. Kunka, and J. V. Small. 1991. Leading edge movement and ulstrastructure in mouse macrophages. *J. Struct. Biol.* 106:1–16.

Runyan, R. B., J. Versakovic, and B. D. Shur. 1988. Functionally distinct laminin receptors mediate cell adhesion and spreading: the requirement for surface galactosyltransferase in cell spreading. *J. Cell Biol.* 107: 1863–1871.

Sabri, S., M. Soler, C. Foa, A. Pierres, A. M. Benoliel, and P. Bongrand. 2000. Glycocalyx modulation is a physiological means of regulating cell adhesion. *J. Cell Sci.* 113:1589–1600.

Shao, J. Y., and R. M. Hochmuth. 1996. Micropipette suction for measuring piconewton forces of adhesion and tether formation from neutrophil membranes. *Biophys. J.* 71:2892–2901.

Sheetz, M. P. 2001. Cell control by membrane-cytoskeleton adhesion. *Nat. Rev. Mol. Cell Biol.* 2:392–396.

Springer, T. A. 1990. Adhesion receptors of the immune system. *Nature*. 346:425–435.

Sykulev, Y., M. Joo, I. Vturina, T. J. Tsomides, and H. N. Eisen. 1996. Evidence that a single peptide-MHC complex on a target cell can elicit a cytolytic T cell response. *Immunity*. 4:565–571.

Tickle, C., and J. P. Trinkaus. 1977. Some clues as to the formation of protrusions by Fundulus deep cells. *J. Cell Sci.* 26:139–150.

Tsai, M. A., R. S. Frank, and R. E. Waugh. 1994. Passive mechanical behavior of human neutrophils: effects of cytochalasin B. *Biophys. J.* 66:2166–2172.

Tsuchiya, S., M. Yamabe, Y. Yamaguchi, Y. Kobayashi, T. Konno, and K. Tada. 1980. Establishment and characterization of a human acute monocytic leukemia cell line (THP-1). *Int. J. Cancer*. 26:171–176.

Verschueren, H. 1985. Interference reflection microscopy in cell biology: methodology and applications. *J. Cell Sci.* 75:279–301.

Vonandrian, U. H., S. R. Hasslen, R. D. Nelson, S. L. Erlandsen, and E. C. Butcher. 1995. A central role for microvillous receptor presentation in leukocyte adhesion under flow. *Cell*. 82:989–999.

Watson, J. M., T. W. Harding, V. Golubovskaya, J. S. Morris, D. Hunter, X. Li, S. Haskill, and H. S. Earp. 2001. Inhibition of the calcium-dependent tyrosine kinase (CADTK) blocks monocyte spreading and motility. *J. Biol. Chem*. 276:3536–3542.

Wülfing, C., M. D. Sjaastad, and M. M. Davis. 1998. Visualizing the dynamics of T cell activation: intercellular adhesion molecule 1 migrates rapidly to the T cell/B cell interface and acts to sustain calcium levels. *Proc. Natl. Acad. Sci. USA*. 95:6302–6307.